Low-Cost Fabrication of Hollow Microneedle Arrays Using CNC Machining and UV Lithography

Hoa Le Thanh, Bao Quoc Ta, Hai Le The, Vy Nguyen, Kaiying Wang, and Frank Karlsen

Abstract—In order to produce disposable microneedles for blood-collection devices in smart homecare monitoring systems, we have developed a simple low-cost scalable process for mass fabrication of sharp-tipped microneedle arrays. The key feature in this process is a design of computer numerical control-machined aluminum sample (CAS). The inclined sidewalls on the CAS enable microfabricated traditional-shaped microneedles (TMNs) to be produced in the desired shape. This process provides significant advantages over other methods that use inclined lithography or anisotropic wet etching. TMNs with a length of 1510 μm, a hollow diameter of 120 μm, and the tip radius of 16 μm were successfully fabricated. Theoretical study and practical measurements of fracture force verified the improved mechanical strength of TMNs for safe skin insertion. In addition, the penetration tests on cadaver pork skin demonstrated that the TMNs could pierce the pork skin without breaking, and create the transport conduits through microneedle lumens. [2014-0361]

Index Terms—CNC machining, UV lithography, SU-8 photoresist, microneedle arrays, fracture force.

I. INTRODUCTION

SAMPLE collection through microfabricated micronee-dles (MNs) has received a great deal of attention in recent years. With several notable advantages of painlessness, minimal invasiveness and self-administration, MNs can serve as an attractive replacement for hypoder-mic needles (HNs) [1], [2]. In healthcare systems, HNs may be the most popular pathway for delivering drugs and collecting blood. However, the dependence on medical specialists, such as doctors or nurses, in using needle related collection of blood is a major obstacle to the development of smart homecare monitoring systems. Another obstacle is the capillary collection tubes that are using large needles that may destroy very small blood vessels. However, very small and very sharp needles may not break or block very small blood vessels. Thus, using microneedle-based devices may be the most effective approach to fulfill this goal. In order to collect blood directly from vessels, in addition to the typical require-ments of sharp tip and hollow structure, microneedle length is required to be longer than 1500μm in order to reach the blood vessels [3], [4]. With that length, fabrication of MNs is very challenging. In this paper, we focus on developing a simple, cheap, and scalable process by exploiting CNC machining and microfabrication technologies to produce TMNs for disposable devices. We have selected microfabricated TMNs for studying because of its unique characteristics such as improved mechanical strength, good sharpness, and large side-opening area.

In the literature, two main approaches were introduced to fabricate TMNs. They are lithographic molding [5] and direct formation of TMNs on the inclined sidewalls [6]–[9]. The first approach provides high possibility to fabricate TMNs with variable tip shapes and a wide range in microneedle materials [5]. However, using lithographic molding, fabrication of long MNs ($\geq 1500\mu$m) is very challenging because of complicated fabrication procedure and the difficulty in performing molding and unmolding processes. On the other hand, the second approach using sidewalls showed a better outcome in microneedle fabrication. With the usage of double-exposure technique, fabrication of MNs on the inclined sidewalls is simpler and more feasible than the first method. Inclined sidewalls is the array of three inclined plane fabricated with a specific angle. The geometry of the inclined sidewalls is very important in defining the shape of beveled tips. Specifically, the tip angle of TMNs is the inclined angle of sidewall. Hence, fabrication of the inclined sidewalls is a crucial step in the fabrication process of TMNs.

To fabricate the inclined sidewalls, two methods have been reported, including anisotropic wet etching of silicon [5]–[7] and SU-8 inclined lithography [8], [9]. However, there are several limitations of these two approaches. First, using anisotropic wet etching can provide high quality silicon sidewalls, such as pyramidal trenches or V-grooves, with very good surface roughness. However, the wet etching procedure is complicated, time-consuming and hard to control accurately the etching depth. Moreover, the dimension of V-groove structures is fixed with the inclined angle of $54.7°$ [10].

H. L. Thanh is with DTU Danchip, Kongens Lyngby 2800, Denmark; also with the Technical University of Denmark, Kongens Lyngby 2800, Denmark; and also with the Buskerud and Vestfold University College, Kongsberg 3603, Norway (e-mail: hoalet@dtu.dk).
B. Q. Ta is with the Division of Computational Mathematics and Engineering, Faculty of Civil Engineering, Institute for Computational Science, Ton Duc Thang University, Ho Chi Minh 2955, Vietnam (e-mail: taquocbao@tdt.edu.vn).
H. L. The is with the Faculty of Civil Engineering, Institute for Computational Science, Ton Duc Thang University, Ho Chi Minh 2955, Vietnam, and also with the MESA+ Institute for Nanotechnology, University of Twente, Enschede 7522 NB, The Netherlands (e-mail: lethehai@tdt.edu.vn).
V. Nguyen, K. Wang, and F. Karlsen are with Buskerud and Vestfold University College, Kongsberg 3603, Norway (e-mail: helen130288@yahoo.com; kaiying.wang@hbv.no; frank.karlsen@hbv.no).
Color versions of one or more of the figures in this paper are available online at http://ieeexplore.ieee.org.
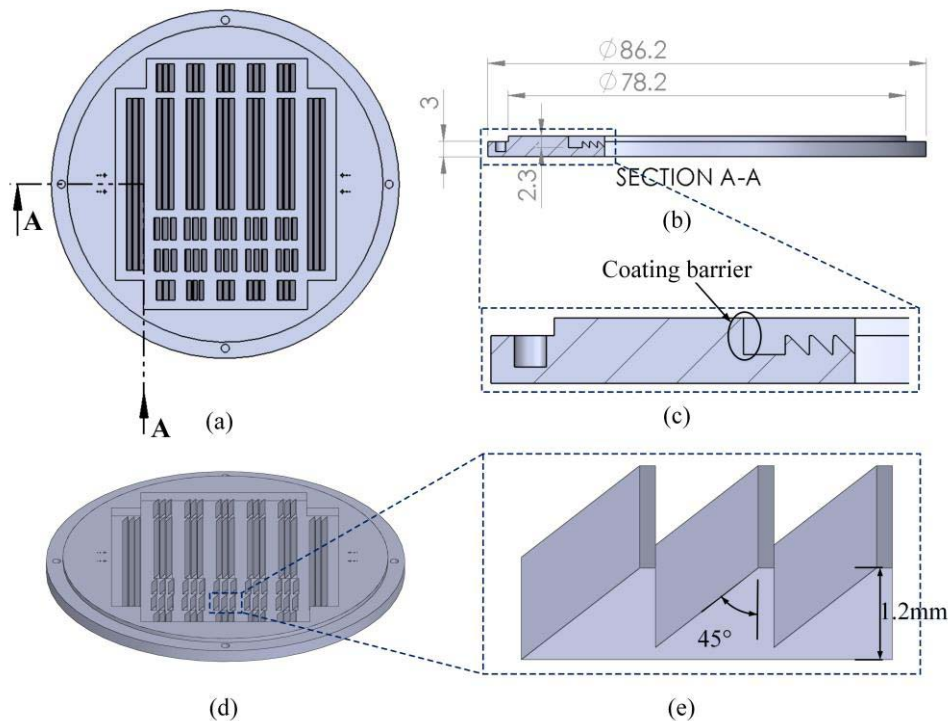Digital Object Identifier 10.1109/JMEMS.2015.2424926

Fig. 1.   Design of CNC- machined aluminum sample (CAS). (a) 3D view of CAS mold, (b) one unit of aluminum inclined sidewalls (AIS), (c) top-view of CAS mold, (d) side-view with cross-sectional view of CAS mold, (e) cross-sectional illustration for coating barrier. All measurements are presented in millimeter as basic unit. The design sketch was drawn in Solidworks 2013.

Second, for inclined lithography, the dimension of SU-8 sidewalls can be varied but still limited. Specifically, although the inclined angle can be increased by changing the incident angle of UV light, the actual angle travelling in SU-8 is decreased due to refraction effect [11]. This effect is resulted from the large refractive index mismatch between SU-8 and air. Light compensation with glycerol is one frequently-used solution [12], [13]. Although this solution can increase the angle by a few degrees, but finding more effective solutions is still desirable.

Furthermore, even when the effect of light refraction on the inclined angle is insignificant, there are still several limitations relating to further steps of SU-8 lithography and double-exposure technique, such as the difficulty in mask alignment, the problems due to thermal deformation of PDMS mold [8], [9]. Thermal deformation of PDMS in baking steps results in a mismatch between the position of microstructures patterned on photomask and the structures on substrate [8]. Re-designing the photomask to compensate such mismatch is one possible solution as reported by Wang et al. [8], [9]. However, mask compensation is not an effective solution for all cases, particularly for different types of photoresist, thickness, heater, etc.

Another approach to fabricate microscale structures follows the current trend of merging Conventional Computer Numerical Control (CNC) machining technology with microfabrication technologies to open a new track in the research and commercialization of complex MEMS-based devices [14]. In general, CNC machining is a well-known manufacturing technology that is easily accessible both in the industry or academic institutions. Because the milling and machining process are controlled numerically by computer, CNC machining technology provides very good repeatability, ultrahigh accuracy and very good tolerance (tens of microns [15], [16]) that lend itself to mass production with significantly lower production cost [17]. For example, Lee et al. [16] demonstrated that complex threedimensional (3D) micromechanical structures can be machined accurately with feature size of 50 μm and the tolerance of 10μm. Another example is the aluminum master molds machined by CNC milling reported by Mecomber et al. [15]. A simple cross-T aluminum template was machined with the channel width of 34.5 μm. These molds were then used to fabricate the polymer-based microfluidic devices by replication process. In brief, CNC machining technology is very promising for use in MEMS-based fabrication. In this paper, the usage of Conventional Computer Numerical Control (CNC) machining technology was exploited to overcome the above-mentioned problems and enable fabrication of inclined sidewalls with variable dimension.

Our aim is to develop a fabrication process that is simpler, faster, and potentially scalable for large-scale production of disposable MNs. A novel design of CNC-machined aluminum sample (CAS) and aluminum inclined sidewalls (AIS) (see Fig. 1) was proposed. Double-exposure technique was used as a core technique to define the TMNs on AIS. Each parameter was optimized during process development. Several problems in the fabrication process were addressed. The performance of the fabricated TMNs was also evaluated. A theoretical study and experimental measurement
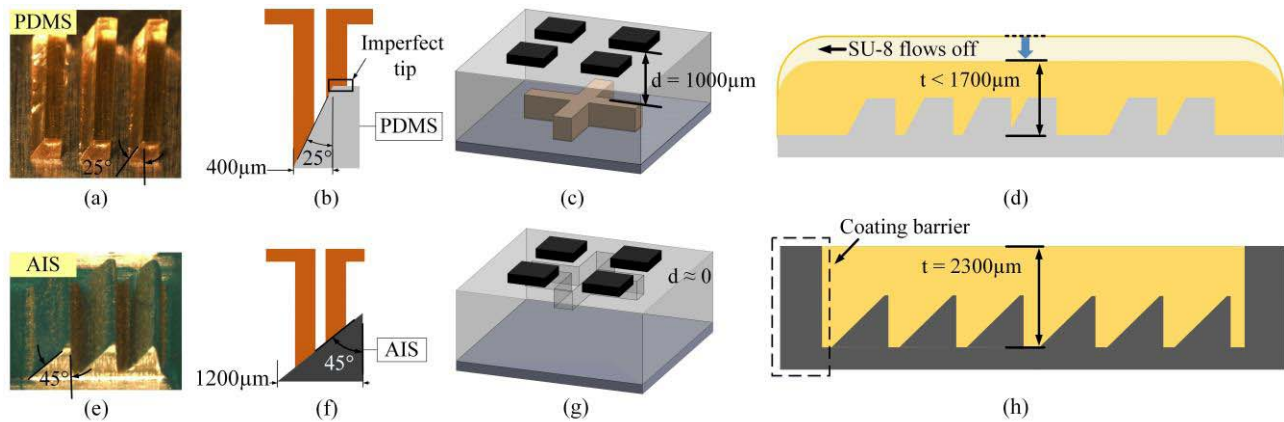
Fig. 2. Schematic illustrations for the problems of the process on PDMS mold and the corresponding solutions provided by the design of CAS mold. (a) optical micrograph of PDMS inclined sidewalls, (b) problem 1: imperfect beveled tips, (c) problem 2: mask alignment error, (d) problem 3: difficulty in coating thick SU-8 layer, (e) optical micrograph of aluminum inclined sidewalls (AIS), (f) solution for problem 1: the usage of wider AIS, (g) solution for problem 2: positioning the alignment marks on the top surface of CAS mold, (h) solution for problem 3: coating barrier.

were conducted to estimate the fracture force of TMNs. Practical performance in terms of the ability to puncture the skin and to transport fluid was checked. Particularly, a microneedle array was inserted into a cadaver pork skin which is the penetration object. A dye stream was then pumped through the lumens by using an external syringe pump. The testing process was carefully inspected under the optical microscope for performance evaluation.

Section 2 describes the work related to the design and manufacturing of CAS mold. Section 3 outlines our experimental work on microneedle fabrication. It presents the development of fabrication process and fabrication results. In Section 4, characterizations of the fabricated TMNs are described, with a focus on the practical performance in terms of mechanical strength, skin penetrability, and fluid transportability. Section 5 presents our conclusion.

II. DESIGN AND MANUFACTURE OF CNC-MACHINED ALUMINUM SAMPLE (CAS)

A 3D design model of CAS mold is depicted in Fig. 1*a*. CAS mold was designed with the outer diameter of 86.2mm and the substrate thickness of 3mm (see Fig. 1*b*). The selected dimension aims to enhance the mechanical strength of the substrate, thus avoid the mold from bending due to thermal expansion. Coating barrier is one important design feature of CAS mold proposed for fabricating long TMNs with controllable length. The illustration of coating barrier is shown in Fig. 1*c*. Since the coating barrier is designed longer in height than AIS, it is expected that the flow of heated SU-8 will not spill out of the edges of CAS mold. Thick SU-8 layer can be coated, enabling to yield long TMNs. In our experiments, coating barriers were machined with three different heights of 1500μm, 1800μm and 2300μm for three CAS molds, respectively. TMNs with the length of 1500μm may be manufacturable with the coating barrier of 2300μm.

The geometry of AIS was designed based on the optimal configuration of microneedle array with 3×3 TMNs and the pitch size of 1500μm. AIS unit was designed with the height of 1.2mm and inclined angle of 45° as depicted in Fig. 1*e*.

The angle of 45° was a compromise between skin penetrability and tip strength. Microneedles with low tip angle, e.g. 15°, have higher skin penetrability, but have lower fracture force; and vice versa. In addition, Fig. 1*d* shows the distribution of 55 AIS units on CAS mold which achieve the throughput of 55 TMNs arrays per process.

It is expected that the design of CAS mold could be the solutions for the problems in the multilayer process on PDMS mold thanks to the mechanical properties of CAS mold, and by some special design features on CAS mold, for example, top-surface alignment marks, coating barrier and variable dimension AIS. In term of the fabrication feasibility and product quality, our approach of using CAS mold has the following advantages over using PDMS mold or silicon V-groove.

A. Higher Inclined Angle of the Needle Tip

Available CNC machining tools are capable of producing AIS with a higher inclined angle and wider sidewalls than lithography or anisotropic silicon wet etching. Wider sidewalls with higher inclined angle may help reduce the imperfection of beveled tips as illustrated in Fig. 2*b*. According to Fresnel's law, the inclined angle of lithographically patterned sidewalls is limited due to a large mismatch in the refractive index between air ($n_{air} = 1$) and SU-8 ($n_{SU-8} = 1.668$ [14]). For example, the actual incident angle of UV light in SU-8 layer is lowered, for example, from 33° to 25° with 900 μm-thick SU-8 layer. The inclined angle of 25° allows the maximum achievable width of 400 μm which is smaller than the diagonal width of the proposed TMNs (420 μm). The beveled tips cannot be formed in the desired shape and results in the problem of imperfection of beveled tips (see Fig. 2*b*). On the other hand, thanks to larger inclined angle, wider AIS can be easily produced. In addition, the usage of CNC machining tools offers more possibility of producing TMNs with a wide range of the tip angle. In this paper, AIS were designed with 45° in inclined angle and 1.2 mm in width (see Fig. 2*f*). This width is about three times wider than 420 μm.
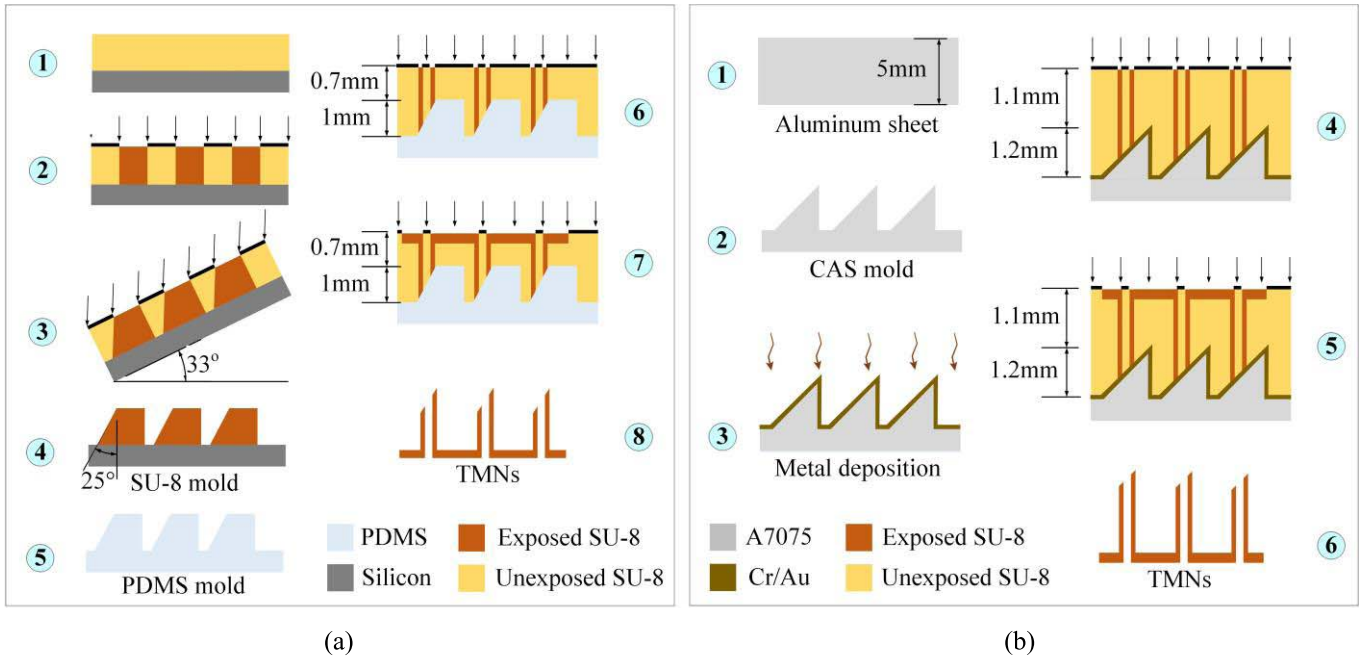
Fig. 3.   Schematic view of the process flows for TMNs fabrication. (a) 3-mask process on PDMS mold. (b) 2-mask process on the proposed CAS mold.

B. Reduced Misalignment

In a multilayer fabrication process, the alignment marks on photomask and PDMS mold are located at different height with a gap of 1mm (see Fig. 2c). Because of this gap, the two marks cannot be focused simultaneously with a built-in optical microscope in mask-aligner. Performing mask alignment is thus very difficult. One possible solution is backside alignment, but the fabrication process would be more complex and cost-inefficient and time-consuming. With CNC machining technology, the alignment marks on the CAS mold can be positioned on the top surface of the mold (see Fig. 2g). The alignment marks on photomask and mold are now close to each other, thus reducing the misalignment. It was experimentally observed that using CAS mold provided higher alignment accuracy than PDMS mold or wet-etched silicon mold.

C. Longer TMNs Can be Fabricated ($\geq 1500 \mu m$) and Easier to Control the Length of TMNs

On the CAS mold, there is a barrier to control the thickness of SU-8 layer, and thus the length of TMNs, as illustrated in Fig. 2h. The height of coating barrier can be up to 2300 μm (Fig. 2h), which is ~600 μm higher than the limited thickness of SU-8 in the traditional fabrication process (Fig. 2d). In fact, with the process on PDMS mold, when the mold is heated beyond SU-8 flow temperature (80 °C or above), SU-8 will reach its viscous liquid flow state and easily flows off the PDMS mold. The volume of SU-8 on PDMS mold will then drop dramatically, resulting in the thickness reduction of SU-8 layer. We experimentally studied that on PDMS mold, the maximum thickness of SU-8 layer is about 1700 μm, which allowing fabrication of $900 \mu m$-long TMNs. On the other hand, in our experiments on CAS molds, 1510 μm-long TMNs were successfully fabricated.

With regard to the manufacture of CAS molds, they were machined by using two machining tools: commercial CNC machine tool V33 (Makino, Japan) and CNC Wire Electrical Discharge Machining (EDM) (PANUC, Japan). The tolerance of these tools is $10 \mu m$. In most of the recent investigations, steel and stainless steel have been widely used as the manufacturing materials [16]. However, these materials would increase significantly the manufacturing time and cost because of its ultra-hardness [15]. Ductile and soft materials such as aluminum or its alloys are desirable for CNC machining in reducing the possibility of tool deformation, thus deteriorating the accuracy and surface roughness of the machined samples [19]. In our research, 5 mm-thick aluminum sheet of aluminum alloy 7075 (A7075) was used as workpiece material to machine CAS molds. The machining procedure can be shortly summarized in three main steps, including: (i) using CNC milling machine to shape the aluminum sheet in vertical direction; (ii) using EDM machine to create the inclination of the AIS with the inclined angle of 45°. In this step, the copper wire with diameter of 5 μm was utilized; (iii) the samples were then polished to obtain the final products. The optical micrographs of CAS mold and AIS units are shown in Fig. 4a and Fig. 5, respectively.

III. Fabrication Process

A. Microneedle Fabrication Process Description

This section describes the fabrication process on CAS mold involving a combination of CNC machining technology, metal deposition and SU-8 UV lithography using a set of two photomasks as shown in Fig. 3. Potential improvements of this process are identified by comparing the proposed process to previous process on PDMS mold [8], [9] in the literature. There are two common stages in both processes, including: fabrication of inclined sidewalls and direct formation

of TMNs. The inclined sidewalls were fabricated by using inclined lithography and CNC machining for the process on PDMS mold and CAS mold, respectively. In the second stage, double-exposure which consists of two exposure steps was used as the key technique. Step 1 aims to define the microneedle shafts and beveled tips on the inclined sidewalls, and step 2 aims to fabricate the baseplates of TMNs arrays.

In general, our CAS mold makes the fabrication of TMNs simpler, faster, more cost-effective and more scalable than the PDMS mold. The usage of industrial micromachining CNC tools to fabricate CAS mold reduce significantly the manufacturing time and cost. The average time for fabricating one CAS mold is remarkably reduced to only about 4-5 hours. On the other hand, fabrication of PDMS mold is more complicated and time-consuming with about 72 hours for fabricating one PDMS mold. Two longest steps in the first process (Fig. 3*a*) are step 1 (soft-baking) and step 5 (PDMS replication). The total time for one process to fabricate TMNs on CAS mold is therefore much faster than on PDMS mold. In addition, with regard to the process flow in Fig. 3*b*, there are some other noticeable advantages, particularly in manufacturing cost. For large-scale fabrication of TMNs array, the amount of SU-8 photoresist used in lithography steps also needs to be considered. In the first process on PDMS mold, about 13g of SU-8 was required for two coating steps (step 1 and 6 in Fig. 3*a*). This number is only about 6g for the proposed process on CAS mold. The cost of making CAS mold is relatively cheaper than that of PDMS mold with the usage of A7075 as machining material. In addition, the cost of making photomasks for fabrication process on CAS mold is lower because the number of needed masks is reduced, that is, two masks in the case of using CAS mold compared to three masks in the cases of using PDMS mold as shown in Fig. 3*b* and in Fig. 3*a*, respectively. The reason behind the increase in the number of needed masks in the process on PDMS mold is that it requires one more mask to perform inclined lithography in step 2 and step 3 in Fig. *3a*. Another considerable problem is the deformation and bending of PDMS substrate caused by thermal expansion during the soft-baking step. This phenomenon leads to a serious problem in misalignment and bad coating profile with high roughness and wrinkles on SU-8 layer which may degrade the quality of TMNs arrays, such as tip sharpness, array configuration or microneedle length, process repeatability, and the overall throughput [8]. Hence, the process on PDMS mold is not suitable for large-scale production of TMNs.

For those reasons, our proposed process on CAS mold could be an efficient method to fabricate TMNs. Simplicity, low manufacturing cost, high throughput, and good repeatability are the most important advantages of the proposed process that lend itself to mass production of disposable TMNs. More importantly, CAS molds can be reusable for further fabrication process only with simple cleaning process.

B. Fabrication of TMNs

Our proposed process consists of six main steps as shown in Fig. 3*b*. They are (i) preparation of aluminum sheet for machining, (ii) manufacture of CAS molds, (iii) deposition of anti-sticking layers (Au/Cr), (iv) coating of SU-8 and step 1 of double-exposure process, (v) step 2 of double-exposure process, and (vi) development of SU-8 and array releasing. Prior to machining of CAS molds, an A7075 workpiece was prepared by cutting into square blocks of 10×10 mm^2 with the thickness of 5 mm. In step 2 in Fig. 3*b*, an A7075 block was machined with three-step procedure to obtain the final machined product of CAS mold. The pre-treatment of CAS mold includes three steps: rinsing with deionized water, cleaning with acetone and isopropanol, and blowing with nitrogen gas. These steps are essential before doing metal deposition. In step 3, thermal evaporator (Moorfield MniLab T25M) was used to deposit two metal layers on the surface of CAS mold to avoid the problem of tip damaging. These layers are 20 nm-thick adhesion layer (Cr) and 50 nm-thick anti-sticking layer (Au). The detailed study on the usage of this layer is presented in next section.

In step 4 in Fig. 3*b*, SU-8 2150 (MicroChem Corp., Newton, MA, USA) was pre-heated at 60 °C in 5 minutes on a Petri dish in order to reduce the viscosity and minimize air bubbles. It was then slowly poured on a CAS mold. The mold was soft-baked on the hot plate at 65 °C for 30 minutes and 95 °C for 15 hours. The hot plate was carefully balance to avoid SU-8 spreading out of the coating barrier. Step 4 and 5 in Fig. 3*b* describe double-exposure technique. In step 4 (first part of double-exposure process), the shafts of TMNs were defined by first photomask. The exposure dosage of 3000mJ/cm^2 was optimally selected. The optical long-pass filter (PL360-LP filter by Omega Opticals) was used because it can eliminate UV radiation below 350nm. By using this filter, the problem of SU-8 absorption was solved, enabling fabrication of long TMNs. The straightness of vertical walls can also be improved.

After step 4, an additional post-baking step was conducted to enhance the contrast between exposed and unexposed regions. Thermal polymerization of exposed SU-8 at microneedle shafts can be accelerated by this baking step. The color of microneedle shafts subsequently turned darker, thus significantly increasing the optical contrast to un-exposed regions. It showed that the alignment process became much easier. Furthermore, baking conditions such as temperature, time, and the type of heater, are very important because repositioning of microneedle shafts may happen. This problem refers to the change in position of exposed microneedle shafts due to the flow of heated SU-8 in the coating layer. This flow results in the position change of microneedle shafts relatively to the sidewalls, thus destroying the configuration of TMNs arrays. The baking parameters were optimized with the usage of convection oven. The baking time was selected to be 2 minutes at 80 °C. It showed that only the top surface was heated, and subsequently turned to liquid state while the bulk region remained solid. Consequently, the shaft position was not changed.

Step 5 (second step of double-exposure process) aims to create the baseplate of TMNs array. In this step, the lumens were covered with the opaque structures on second photomask

to avoid blocking of lumens. To ensure the protection for lumens, mask alignment is very important. 300 μm-thick base plates were successfully fabricated by using low exposure dosage (300 mJ/cm^2).

In step 6 in Fig. 3*b*, the sample was developed in developer mr-Dev 600 for 10 minutes with ultrasonic agitation (Ultrasonic Cleaning Brandson 3100). The arrays were automatically released from CAS mold. The released arrays were then collected by using metallic tweezers. To completely open the lumens, an additional 2-min development was required. The arrays were then gently blown dry using a nitrogen gun. Finally, a flood exposure step (2000 mJ/cm^2 exposure dosage) and hard bake (130 °C for 5 minutes) were conducted to enhance the mechanical strength of TMNs.

After the fabrication process, a cleaning procedure was necessary to prepare the CAS molds for further fabrication experiments. The CAS molds were firstly cleaned with ultrasonic agitation in SU-8 developer mr-Dev 600 or SU-8 removal to remove the residual SU-8. The molds were then rinsed with deionized water, acetone, and isopropanol before being blown dry using nitrogen gun. Plasma cleaning (Plasma Cleaner Addax 3031) was the last step of the cleaning process. In fact, the cost of these cleaning processes is much less than that of machining a new CAS mold. This is because these processes used cheap and accessible chemicals. They are standard cleaning procedures in micro-fabrication technologies. Moreover, deposition of anti-sticking layers is required for new CAS molds. When using CAS mold, reusability is thus one of the most important advantages.

C. Avoiding Tip Damaging and the Usage of Anti-Sticking Layer

Tip damaging may happen during releasing TMNs from the CAS mold. One possible reason is the strong adhesion between aluminum surface and cured SU-8, subsequently causing damage to the beveled tips. After releasing, the beveled tips were still remained on the surface of AIS. Moreover, fabricating TMNs using the original CAS mold normally requires a long developing step ($>$2 hours) in order to achieve full development of microneedle lumens. However, long development time results in significant bending of baseplates as reported by Wang [20]. The development time therefore has to be reduced to minimize the possibility of baseplate bending while ensuring that the lumens are fully developed. Hence, reducing the adhesion between cured SU-8 and CAS mold is very important.

Our solution is to use an anti-sticking layer for easier separation of MNs. The material of this layer was carefully considered in relation to two aspects of its adhesion to cured SU-8 and deposition technologies. For anti-sticking layer, it is required that this layer has low adhesion with cured SU-8, and strong adhesion with CAS mold. The selection of materials was based on an experiment conducted on a CAS mold. The results obtained from this experiment are vital to the development of a full process for efficiently fabricating TMNs. In this experiment, the surface of a CAS mold was divided
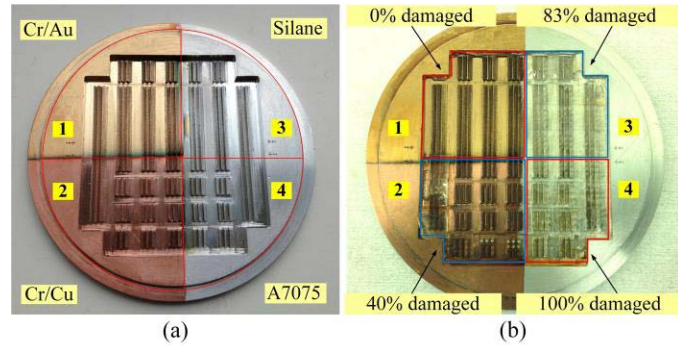

Fig. 4. Optical micrographs of CAS mold. (a) four quarter regions on CAS mold, coated with Au, Cu, Silane and the original surface of CAS mold, (b) microneedle arrays in four quarter regions after 10-minute development with ultrasonic agitation.
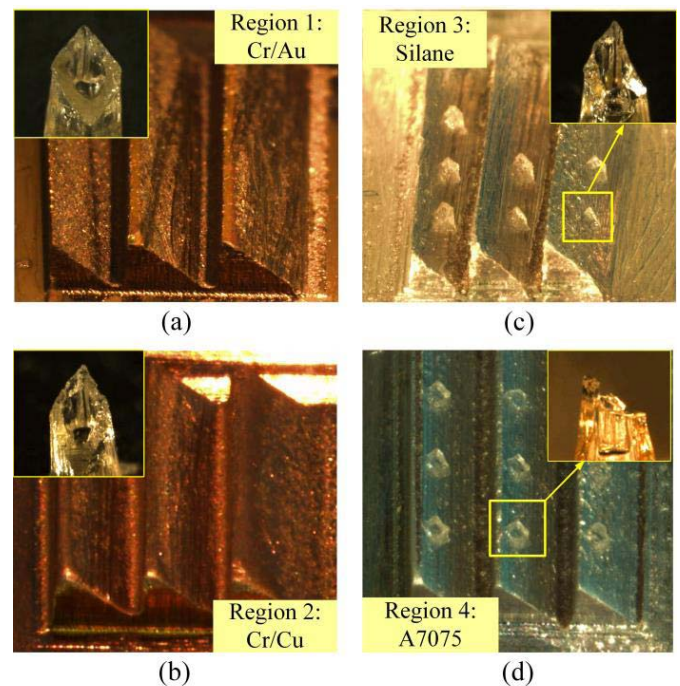

Fig. 5. Optical micrographs of AIS coated with anti-sticking layer (a) 20 nm Cr and 20 nm Au, (b) 20nm Cr and 500nm Cu, (c) silane, (d) original aluminum (A7075) surface.

into four quarter regions as shown in Fig. 4. Gold (Au), copper (Cu), and Silane layers were coated on region 1, 2, and 3 of aluminum CAS mold as anti-sticking layers, respectively. Region 4 was the original aluminum surface of CAS mold. Moreover, a chrome (Cr) layer was used as an adhesion layer (in regions 1 and 2) to enhance the adhesion between an anti-sticking layer and CAS mold.

With regard to deposition technology, thermal evaporator was selected because of its advantages over traditional spin coating. These advantages are high uniformity of coated metallic layer, simple, and inexpensive process. Spin coating cannot be used since the surface of CAS mold is not flat with numbers of AIS units. The spun layer therefore cannot be uniformly deposited, thus the surface of CAS mold may not be fully covered. In our experiment,
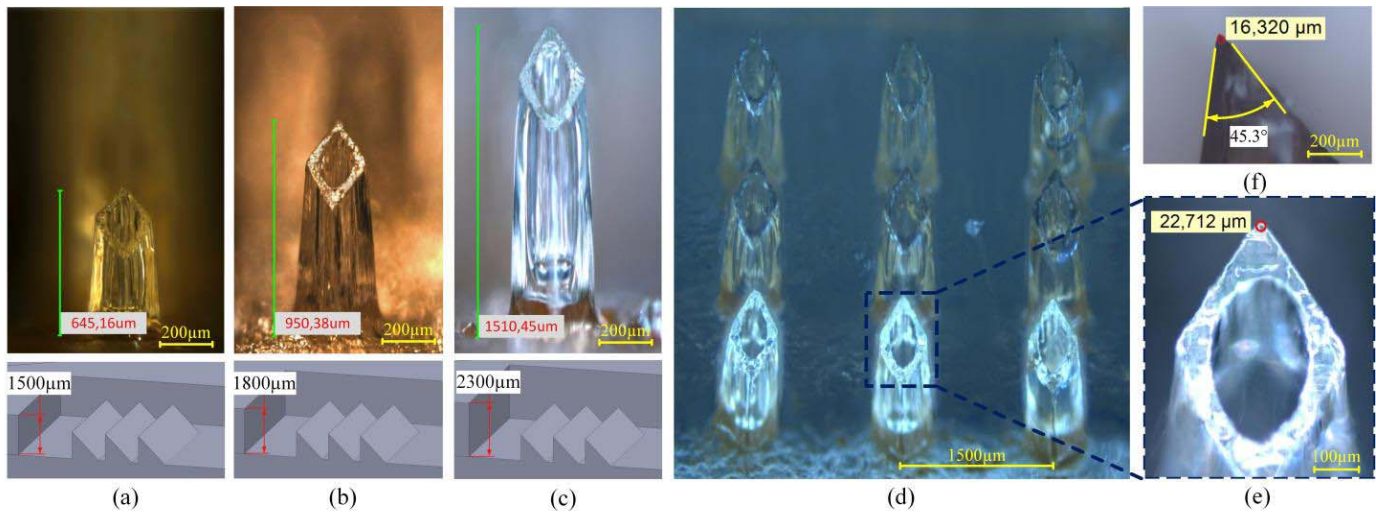
Fig. 6. Optical micrographs of fabricated TMNs. (a) 645μm-long TMNs, (b) 950μm-long TMNs, (c) 1510μm-long TMNs. (d) an array of 3×3 1510μm-long TMNs fabricated with the pitch size of 1500μm, (e) front-view and (f) side-view of the fabricated beveled tip. The thickness of the base plate was measured to be approximately 300μm with the exposure dosage of 300mJ/cm2.

TABLE I

THE EXPERIMENTAL DATA OF A STUDY ON MATERIAL SELECTION FOR ANTI-STICKING LAYER

Materials	Damaged arrays (%)	Separation method	Baseplate condition	Development time (minutes)
Cr/Au	0% (0/15)	100% self-released	100% flat	10
Cr/Cu	40% (6/15)	60% self-released	50% flat	15
Silane	83% (10/12)	metallic tweezers	100% bended	120
Al	100% (12/12)	metallic tweezers	100% bended	120

thermal evaporator (Moorfield MiniLab T25M) was used for metal deposition.

The performance of each material was evaluated based on four criteria, i.e., percentage of damaged arrays, separation method, the flatness of the baseplate and development time. This experiment was repeated three times and the results are presented in Table I.

It is demonstrated that region 1 coated with Cr/Au showed a better performance over other regions. 100% TMNs arrays were self-released in good condition without baseplate bending or lumen blocking. Specifically, there was no damaged arrays observed in region 1 (see Fig. 5a) when all the arrays were automatically released during the development process. In addition, the lumens were completely opened after 10-minute development with ultrasonic agitation. In fact, as the arrays were released, the developer SU-8 inside the lumens is accelerated, thus reducing the time to obtain full development. On the other hand, the percentage of damaged arrays on region 2 and 3 were 40% and 83%, respectively, as shown in Fig. 4b and Table I. For region 4, all arrays were remained on CAS mold after 120-minute development. Those arrays had to be released manually by using metallic tweezers. After this process, there remained residues on the sidewalls (see Fig. 5c, d), indicating that the tips were damaged.

For those reasons, Au has been selected as a potential material for anti-sticking layer, which is coated on the surface of CAS molds to reduce the adhesion between SU-8 and CAS mold. This layer helps to solve the problem of tip damaging and enable the fabrication of desired beveled tips.

IV. CHARACTERIZATION OF FABRICATED TMNs

This section describes the characterization of the TMNs arrays, with emphasize on mechanical strength, skin penetrability, and fluid transportability.

A. Fabricated TMNs

In our experiment, microneedle fabrication was conducted on three CAS molds with the expectation of being able to control the microneedle length. Fig. 6a, b, c show the optical micrographs of TMNs fabricated with a length of 645μm, 950μm, and 1510μm corresponding to the coating barrier of 1500μm, 1800μm, and 2300μm, respectively. TMNs with a width of 300μm and diameter of 120μm were successfully fabricated.

In addition, Fig. 6d illustrates an array of 3×3 1510 μm-long TMNs fabricated with the pitch size of 1500 μm. The optical micrographs of beveled tip are shown in Fig. 6e, f. The opening of the fabricated TMNs can be observed in Fig. 6e which shows the front-view micrograph. The beveled tips were successfully fabricated as compared to the proposed design with small variation, that is, tip angle of 45.3° (see Fig. 6f). In addition, good sharpness was achievable with the tip radius ranges from 16 μm to 22 μm as depicted in Fig. 6e. The fabrication results verified the expected outcomes of our proposed process on CAS mold. TMNs were manufacturable with the desired length, shape, and tip radius. The results indicate that this process is scalable for large-scale manufacturing of SU-8 TMNs.

B. Mechanical Strength of the Fabricated TMNs

Both theoretical calculation and experimental measurements of the fracture force was conducted. A microneedle must have a high fracture force to ensure safe skin penetration.

TABLE II
FRACTURE FORCES MEASUREMENT OF FABRICATED SU-8 TMNs

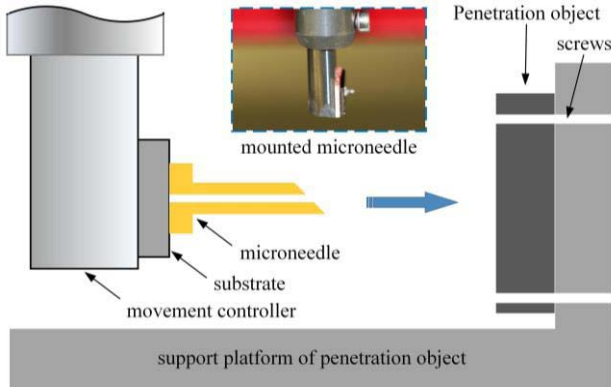| Length (μm)	Measured force (N)		Calculated force (N)	Length reduction (μm)	Increased force (shaft) (N)
	Tip	Shaft	Shaft		
650	0.62	3.45	3.05	97	3.24
950	0.51	2.89	2.56	120	2.72
1510	0.53	2.41	1.84	105	2.11
			APD = 17.1%		APD = 8.3%

Fig. 7. Schematic drawing of equipment setup for measuring fracture force. A TMN was mounted on a 3mm-square silicon substrate. A 1mm-thick aluminum plate (A7075) was utilized as penetration object. A support platform was used to stabilize the penetration object using four screws. The movement controller moved in horizontal direction i.e. blue arrow direction.

Fig. 8. A force-time plot obtained from the measurement of a 1510μm-long traditional-shaped microneedle.

In fact, fracture force has to be significantly higher than the insertion force, which is the minimum force required to puncture the skin. We utilized a theoretical model to estimate the critical buckling load (P_{cr}), applying for structural objects with variable cross-sectional area. This mathematical expression of this model was firstly introduced by Smith [21] as presented in (1).

$$P_{cr} = \frac{E\pi^2}{2L^3} \int_0^L \sum_{i=0}^n I(z) . \cos^2\left(\frac{\pi z}{2L}\right) dz \qquad (1)$$

where P_{cr} is the critical buckling load, $I(z)$ is the second moment of area, E is the Young's modulus and L is the effective length of the microneedle. The calculations were done by using Maple. The computational results are shown in Table II.

The theoretical prediction of P_{cr} was verified by the practical measurement of fracture force using Shear Tester Delvotec 5600. The schematic diagram of the measurement setup is shown in Fig. 7. The measurement was conducted on individual TMN. A microneedle was fixed on the substrate, and then mounted to the movement controller. The movement of microneedle was precisely controlled by a built-in motor which has the resolution of 0.01N. A rigid surface (1 mm-thick aluminum plate, Young's modulus of 69GPa) served as a penetration object. This plate was then covered by a thin layer of epoxy resin UN3082. This layer provided a softer surface to immobilize the microneedle tip during measurement, thus minimizing the measurement error due to slippery effect.
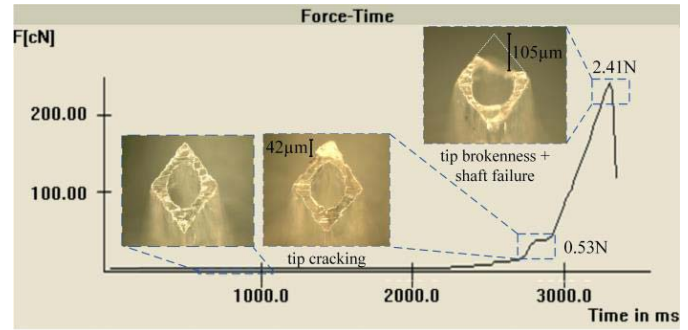
The applied force was recorded as a function of movement time. The force-time relation obtained from the measurement is shown in Fig. 8. In this plot, there are two critical points of brokenness, i.e. tip cracking at 0.51 N and shaft failure at 2.41 N. This implies that the beveled tip was firstly cracked with a length reduction of 42 μm. The beveled tip was hardly damaged at the force of 2.41 N, causing a length reduction of 105 μm. At this point, the tested TMNs was broken at its bottom part and separated from the baseplate. This type of brokenness is called shaft failure. The mechanism of this failure mode is what described by a theoretical model above. The comparison of calculated forces and measured forces are shown in Table II.

We conducted five measurements for each of three types of TMNs fabricated with different lengths. The average fracture forces were recorded and presented in Table II. The measured forces at tip-cracking were 0.53 N, 0.51 N and 0.62 N corresponding to length of 1510 μm, 950 μm, and 645 μm, respectively. It can be seen that the tip-cracking forces for all TMNs types were comparable with a small variation of 0.11 N. This variation is due to a small difference in the radii of beveled tips, which ranged from 16 μm to 22 μm (see Fig. 6e, f). On the other hand, there was a dramatic increase in the shaft-failure forces when length decreased. They were measured to be 2.41 N, 2.89 N, and 3.45 N corresponding to the length of 1510 μm, 950 μm, and 645 μm, respectively. The results demonstrated that TMNs can bare smaller force with longer length.

Table II gives a comparison between the theoretically predicted fracture forces and measured fracture forces. The average percentage difference (APD) is 17.1%. The reason for this difference could be the reduction of length when the tip is broken. For example, for 1510 μm-long TMNs, the length was reduced by 105 μm from 1510 μm to 1405 μm. Due to the length reduction, the mechanical strength of TMNs increases and the fracture force is higher. To calculate the increased P_{cr}, the amount of length reduction was taken into account in the theoretical model. The measured results then show a better agreement, i.e. the APD of 8.3%, with theoretically calculated P_{cr}.

The discussion on safe skin penetration of the fabricated TMNs is given below. We compared the fracture forces of fabricated TMNs to the forces to insert microneedles into skin.
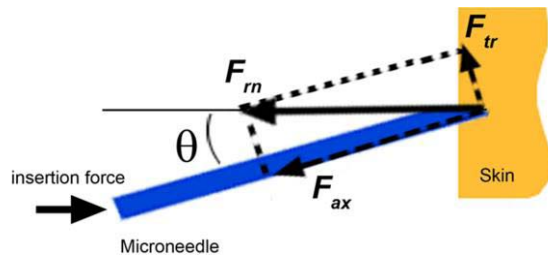
Fig. 9. Schematic illustration of forces acting on a microneedle when inserting non-perpendicular to the skin surface. F_{rn} denotes the net reaction force of the skin to the microneedle. F_{tr} denotes the transverse component of F_{rn}, and F_{ax} denotes the component along the microneedle axis.

For the practical use on human subjects, the skin piercing pressure is about 3.18 MPa (3.18×10^6 N/m^2) [22]. However in practice, the skin always deforms before being punctured. According to Kong et al. [23], at this puncturing point, the maximum skin deformation is about 152 μm. For the proposed beveled tip, the force applying area was calculated to be 3.26×10^{-8}m^2. The insertion force can be calculated to be 0.104 N by multiplying the skin piercing pressure to the force applying area. Average tip-cracking forces (0.53 N for 1510 μm-long TMNs) were generally five times larger than the forces needed to insert microneedles into skin, indicating that the fabricated TMNs could pierce skin without breaking. Safe skin penetration therefore may be at hand.

In practice, there is probably a small deviation from 90° of the insertion angle which causes TMN microneedle to bend due to the bending force, i.e. the transverse component of the reaction force from the skin to the microneedle. Considering the bending fracture, an analytical model developed in [24] based on maximum shear stress condition is used to calculate the maximum bending force that causes fracture of the microneedle. Applying this model for our TMNs, the bending fracture force is calculated to be $\sim$0.063 N at an insertion depth of 152 μm. For skin piercing, the axial component of insertion force, and thus the axial component of the reaction force from the skin to the microneedle (F_{ax}), should be at least 0.104 N, as explained in the previous paragraph. The transverse component of the reaction force is calculated as $F_{tr} = F_{ax} \times tan(\theta)$, where θ is the deviation angle (see Fig. 9). When F_{ax} = 0.104 N, a deviation angle θ of 20° leads to F_{tr} = 0.037 N, which is well below the limit 0.063 N. Therefore, a small deviation in the insertion angle is not likely to cause fracture of TMN microneedle.

C. Skin Penetrability and Fluid Transportability

In our experiment, we also studied skin penetrability and fluid transportability of fabricated TMNs arrays. Specifically, TMNs arrays were used to pierce the cadaver pork skin followed by pumping of testing liquid through the needle lumens in a manner similar to delivery drug with HNs.

The integration of TMNs array is depicted in Fig. 10. The microneedle array was connected to the fluidic connection via a PDMS microfluidic connection. This connection was designed with circular cavity at the bottom, connecting to the backside of array. The array was then connected to the syringe pump via a 3mm-diameter polymer tube integrated in the
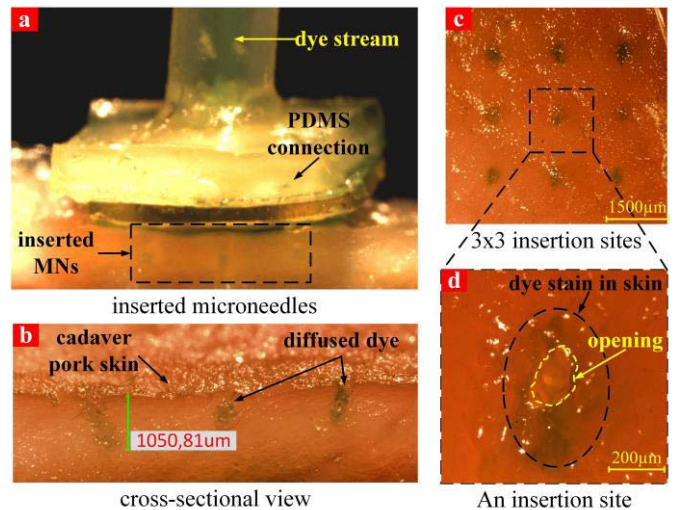

Fig. 10. Optical micrographs of a penetration test on the cadaver pork skin. (a) pumping of dye stream through inserted TMNs into cadaver pork skin, (b) cross sectional view of insertion sites with retained dye, (c) top view of insertion sites, (d) measurement of an insertion site. This test was inspected by using an optical microscope (Olympus MVX10, Hamburg, Germany).

other side of PDMS connection. A syringe pump (Model 100, Kd Scientific Inc., MA, USA) was used to generate pumping pressure. An approximate pressure of 5 KPa was applied to drive the stream of testing liquid. In this experiment, the testing liquid was a mixture of black-green dye and DI water with the proportion of 1:5, respectively. The cadaver pork skin was used as the penetration object.

The testing procedure is now described. The 1510 μm-long TMNs array was inserted by pressing vertically down to the cadaver pork skin. The inserted TMNs are shown in Fig. 10a. When the array was inserted, syringe pump drove the dye stream through the inserted TMNs to the cadaver pork skin. As the penetration depth reached about two third of the total length, an array was gently pulled out and finish the test. The results are shown in Fig. 10. The practical performance of TMNs array was evaluated based on two aspects, including skin penetrability and fluid transportability.

First, skin penetrability refers to the ability of MNs to pierce the skin without breaking. In general, skin penetrability depends on several factors, for example: tip shape, tip radius and the configuration of microneedle array (i.e. number of needles and the pitch size). In this test, microfabricated TMNs with a tip radius of 16 μm, tip angle of 45° arranged in 3×3 array was used. The results illustrated that TMNs arrays with the pitch size of 1500 μm may be able to overcome the backpressure against nine needles and puncture the pork skin. All the TMNs on the arrays could pierce the outer barrie 10-15 μm of skin, called stratum corneum, and easily reach to the deeper layers. The insertion depth and the width of opening site were measured to be 1050 μm and 180 μm as shown in Fig. 10b and Fig. 10d, respectively. During the penetration step, brokenness or significant deformation of beveled tips was not observed. This indicates that the fabricated TMNs were strong and sharp enough to puncture the pork skin.

Second, fluid transportability is the ability to create the transport conduits for drug delivery or blood collection through the microneedle lumens. This ability depends on the successful

fabrication of the lumens in hollow TMNs. If the lumens are blocked, the TMNs arrays will not work and the process to fabricate hollow TMNs cannot be used. To verify fluid transportability, after inserting the TMNs into the pork skin, a dye stream was pumped through the lumens of inserted TMNs by using a syringe pump. The infusion of testing liquid at the polymer tube and the microneedle lumens can be inspected in Fig. 10a. The dye stream was successfully driven through the lumens, and diffused into the pork skin. From Fig. 10a, c, it can be seen that dye still stained viable epidermis underneath after the array was pulled out. This indicates that the hollow lumens were successfully fabricated and our TMNs arrays could create conduits for fluid transport.

V. Conclusion

A simple, robust fabrication process, scalable for cheap and reproducible mass production of SU-8 traditional-shaped microneedles (TMNs) has been reported in this paper. Our key finding is the usage of CNC-machined aluminum sample (CAS) that facilitates the fabrication of TMNs. A CAS mold yields 55 arrays of TMNs per process, and it is reusable. We have found that the CAS mold is a solution for the following limitations and problems: small inclined angle for the tip, alignment error, substrate bending and deformation, and some problems in fabricating long TMNs ($\geq$1500 μm) of reported approaches in literature that use inclined lithography or anisotropic wet etching.

Our proposed process has several advantages for microneedle fabrication over reported processes in literature. Our process is simpler and faster, more reliable, and more cost-effective. In addition, our process enables the fabrication of very long TMNs (1510 μm). The lithography process is greatly simplified with one lithography step, thus reducing the manufacturing time and cost by using less chemical consumption and photomasks. The CAS mold can be cleaned and reused for another fabrication batch. The penetration tests on cadaver pork skin showed that the fabricated TMNs have good mechanical strength for safe skin penetration. The existence of hollow lumens was verified by the experiments on fluid transportability. Our simple, low-cost and robust fabrication process may be thus suitable for mass production of disposable TMNs.

References

[1] R. K. Sivamani, B. Stoeber, G. C. Wu, H. Zhai, D. Liepmann, and H. Maibach, "Clinical microneedle injection of methyl nicotinate: Stratum corneum penetration," *Skin Res. Technol.*, vol. 11, no. 2, pp. 152–156, May 2005.

[2] J. W. Lee, J.-H. Park, and M. R. Prausnitz, "Dissolving microneedles for transdermal drug delivery," *Biomaterials*, vol. 29, no. 13, pp. 2113–2124, May 2008.

[3] B. P. Chaudhri, F. Ceyssens, P. D. Moor, C. Van Hoof, and R. Puers, "A high aspect ratio SU-8 fabrication technique for hollow microneedles for transdermal drug delivery and blood extraction," *J. Micromech. Microeng.*, vol. 20, no. 6, p. 064006, 2010.

[4] C. G. Li, C. Y. Lee, K. Lee, and H. Jung, "An optimized hollow microneedle for minimally invasive blood extraction," *Biomed. Microdevices*, vol. 15, no. 1, pp. 17–25, Feb. 2013.

[5] R. Lüttge *et al.*, "Integrated lithographic molding for microneedle-based devices," *J. Microelectromech. Syst.*, vol. 16, no. 4, pp. 872–884, 2007.

[6] S.-C. Kuo and Y. Chou, "A novel polymer microneedle arrays and PDMS micromolding technique," *Tamkang J. Sci. Eng.*, vol. 7, no. 2, pp. 95–98, 2004.

[7] F. Ceyssens, B. P. Chaudhri, C. Van Hoof, and R. Puers, "Fabrication process for tall, sharp, hollow, high aspect ratio polymer microneedles on a platform," *J. Micromech. Microeng.*, vol. 23, no. 7, p. 075023, 2013.

[8] P.-C. Wang, S.-J. Paik, S. Chen, S. Rajaraman, S.-H. Kim, and M. G. Allen, "Fabrication and characterization of polymer hollow microneedle array using UV lithography into micromolds," *J. Microelectromech. Syst.*, vol. 22, no. 5, pp. 1041–1053, Oct. 2013.

[9] P.-C. Wang, S.-J. Paik, S.-H. Kim, and M. G. Allen, "Hypodermic-needle-like hollow polymer microneedle array: Fabrication and characterization," *J. Microelectromech. Syst.*, vol. 23, no. 4, pp. 991–998, Aug. 2014.

[10] M. J. Madou, *Fundamentals of Microfabrication: The Science of Miniaturization*. Boca Raton, FL, USA: CRC Press, 2002.

[11] M. Han, W. Lee, S.-K. Lee, and S. S. Lee, "3D microfabrication with inclined/rotated UV lithography," *Sens. Actuators A, Phys.*, vol. 111, no. 1, pp. 14–20, Mar. 2004.

[12] K.-Y. Hung, H.-T. Hu, and F.-G. Tseng, "Application of 3D glycerol-compensated inclined-exposure technology to an integrated optical pick-up head," *J. Micromech. Microeng.*, vol. 14, no. 7, p. 975, 2004.

[13] K.-Y. Hung and T.-H. Liang, "Application of inclined-exposure and thick film process for high aspect-ratio micro-structures on polymer optic devices," *Microsyst. Technol.*, vol. 14, no. 9–11, pp. 1217–1222, Oct. 2008.

[14] K. F. Ehmann, R. E. DeVor, and S. G. Kapoor, "Micro/meso-scale mechanical manufacturing—Opportunities and challenges," in *JSME/ASME Int. Conf. Mater. Process.*, vol. 1. Oct. 2002, pp. 6–13.

[15] J. S. Mecomber, D. Hurd, and P. A. Limbach, "Enhanced machining of micron-scale features in microchip molding masters by CNC milling," *Int. J. Mach. Tools Manuf.*, vol. 45, no. 12–13, pp. 1542–1550, Oct. 2005.

[16] L. J. Lee *et al.*, "Design and fabrication of CD-like microfluidic platforms for diagnostics: Polymer-based microfabrication," *Biomed. Microdevices*, vol. 3, no. 4, pp. 339–351, Dec. 2001.

[17] W. T. Lei, M. P. Sung, W. L. Liu, and Y. C. Chuang, "Double ballbar test for the rotary axes of five-axis CNC machine tools," *Int. J. Mach. Tools Manuf.*, vol. 47, no. 2, pp. 273–285, Feb. 2007.

[18] S. K. Mitra and S. Chakraborty, *Microfluidics and Nanofluidics Handbook: Fabrication, Implementation, and Applications*. Boca Raton, FL, USA: CRC Press, 2011.

[19] Y. Takeuchi, K. Miyauchi, K. Morishige, and N. Asakawa, "Six-axis control grooving by means of ultrasonic vibrational cutting," in *Proc. 2nd Int. Seminar Improving Mach. Tool Perform.*, Jul. 2000, p. 22, paper CD-ROM.

[20] P.-C. Wang, "Fabrication, packaging, and application of micromachined hollow polymer needle arrays," Ph.D. dissertation, School Elect. Comput., Georgia Inst. Technol., Atlanta, GA, USA, 2013, p. 69.

[21] W. G. Smith, "Analytic solutions for tapered column buckling," *Comput. Struct.*, vol. 28, no. 5, pp. 677–681, 1988.

[22] M. W. Ashraf, S. Tayyaba, N. Afzulpurkar, and A. Nisar, "Fabrication and analysis of tapered tip silicon microneedles for MEMS based drug delivery system," *Sensors Transducers J.*, vol. 122, no. 11, pp. 158–173, Nov. 2010.

[23] X. Q. Kong, P. Zhou, and C. W. Wu, "Numerical simulation of microneedles' insertion into skin," *Comput. Methods Biomech. Biomed. Eng.*, vol. 14, no. 9, pp. 827–835, 2011.

[24] H. L. Thanh, H. L. The, V. Nguyen, N. Tran-Minh, K. Wang, and F. Karlsen, "Optimal design of polymer-based microneedle for improved collection of whole blood from human fingers," *Micro Nano Lett.*, vol. 9, no. 10, pp. 644–649, 2014.

Hoa Le Thanh received the B.S. degree in electronics and telecommunications engineering from the Ho Chi Minh City University of Technology, Vietnam, in 2012, and the M.S. degree in micro and nanosystem technology from Buskerud and Vestfold University College, Norway, in 2014. He is currently pursuing the Ph.D. degree in electronics, communications, and space engineering with the Technical University of Denmark, Kongens Lyngby, Denmark. His current research interests include engineering of passive electronic components for power supply. His other research interests include microfluidic devices for clinical applications, photonic biosensors, and nanowire-based biosensors.

Bao Quoc Ta received the B.Sc. degree from the École Central de Paris and the Ho Chi Minh City University of Technology, and the M.Sc. and Ph.D. degrees from Buskerud and Vestfold University College, Norway. Since 2008, he has been very active in the field of local synthesis and direct integration of carbon nanotubes into microsystems for sensor applications. In 2009 and 2011, he was a Visiting Researcher with Linlab, the laboratory of Prof. L. Lin, Berkeley Sensors and Actuators Center, University of California, Berkeley, CA, USA. He is currently with the Institute for Computational Science, Ton Duc Thang University, Vietnam, with a focus on computational micro and nanotechnology. He received the first prize in the competition of Innovation for Future Nanotechnology by the Research Council of Norway in 2011.

Hai Le The received the B.E. (Hons.) degree in electronics and telecommunications engineering from the Ho Chi Minh City University of Technology, Vietnam, in 2012, and the M.S. degree in micro and nanosystems technology from Buskerud and Vestfold University College, Norway, in 2014. He is currently pursuing the Ph.D. degree in nanotechnology with the MESA+ Institute for Nanotechnology, University of Twente, The Netherlands. He has been a Researcher (five months) with the Institute for Computational Science, Ton Duc Thang University, Vietnam. His major interests are micro/nanofabrication, micro/nanofluidics, catalytic reactions, and ceramic materials. His other research interests include fluid mechanics, modeling and simulation, and image processing algorithm.

Vy Nguyen received the B.S. degree in electronics and telecommunications engineering from the Da Nang University of Technology, Vietnam, in 2012, and the M.S. degree in micro and nanosystem technology from Buskerud and Vestfold University College, Norway, in 2014. Her current research interests include BioMEMS, microfluidics, nanobiotechnology, and their biomedical applications.

Kaiying Wang received the M.Sc. degree in inorganic chemistry from Northwest University, in 1992, and the Ph.D. degree in condensed matter physics from the Institute of Physics, Chinese Academy of Sciences, in 1995. He joined the Department of Micro/Nano Systems Technology, Buskerud and Vestfold University College, in 2007, as an Associate Professor, and was promoted to Professor in 2010. He has authored over 90 scientific papers in international journals and conferences in materials science. His research interests are focused on microfabrication and nanotechnology, functional thin films, polymer materials, nanostructure characterization, and nanodevices for environment and energy applications.

Frank Karlsen received the M.Sc. degree in biotechnology from the Chemistry Institutes, Norwegian University of Science and Technology, Trondheim, Norway, in 1988; the Ph.D. degree in molecular pathology and biology from the Institutes of Cancer Research, University of Oslo, Norway, in 1997; and the Ph.D. degree in environmental microbiology from the Institutes of Microbiology, University of Oslo, in 1999. He was a Scientific Assistant (14 months) in the clinical microbiology with ST Olav's Hospital, Trondheim. He was a Scientist (six years) with the Department of Pathology, Norwegian Radium Hospital, Norway. He was a Product Specialist (one year) with Organon Technica, Asker, Norway. He was the Chief Scientific Officer (14 years) of NorChip AS. He was a Professor II with Vestfold University College, Norway, from 2008 to 2010. He has being employed as a Professor with Buskerud and Vestfold University College, Tonsberg, Norway, since 2010.